Redox-behavior and reactivity of formazanate ligands

Mondol, Ranajit

DOI:
10.33612/diss.107969043

Chapter 3

Reactivity of 2-electron reduced formazanate boron compounds with electrophiles: Facile N-H/N-C bond homolysis due to formation of stable ligand radicals

The reactivity of a boron complex with redox-active formazanate ligand, $LBPh_2$ (L = PhNNC(*p-tol*)NNPh), was studied. Two-electron reduction of this main group complex generates the stable, nucleophilic dianion $[LBPh_2]^{2-}$, which reacts with the electrophiles BnBr and H_2O to form products that derive from ligand benzylation and protonation, respectively. The resulting complexes are anionic boron analogues of leucoverdazyls. N-C and N-H bond homolysis of these compounds was studied by exchange NMR spectroscopy and kinetic experiments. The weak N-C and N-H bonds in these systems derive from the stability of the resulting borataverdazyl radical, in which the unpaired electron is delocalized over the four nitrogen atoms in the ligand backbone. We thus demonstrate the ability of this system to take up two electrons and an electrophile ($E^+ = Bn^+, H^+$) in a process that takes place on the organic ligand. In addition, we show that the [$2e^-/E^+$] stored on the ligand can be converted to $E^\bullet$ radicals, reactivity that has implications in energy storage applications such as hydrogen evolution.

This chapter has been published:

R.Mondol and E.Otten* "Reactivity of 2-electron reduced formazanate boron compounds with electrophiles: Facile N-H/N-C bond homolysis due to formation of stable ligand radicals" *Inorg. Chem.,* **2018**, 57, 9720–9727.

3.1 Introduction

A key feature in the reactivity of molecular complexes with transition metal centers is their ability to change oxidation states via electron-transfer reactions. This has allowed the development of a large variety of redox-based catalytic transformations that are of importance in the synthesis of organic molecules, polymers and materials. Often these reactions rely on 2-electron steps (e.g., oxidative addition / reductive elimination). Also in energy applications, interconversion between redox-states in simple small molecules is relevant, and catalysis is imperative to allow high reaction rates and to control product selectivity. With the transition from a fossil-based to a renewable energy supply, a key challenge is to develop reliable, cheap methods to convert and store sustainable energy into chemicals ('solar fuels').[1] Examples of chemical reactions for energy storage include CO_2 reduction to CO, formatic acid or methanol,[2] the interconversion between dinitrogen and ammonia,[3] and water splitting.[4] In the latter, the oxidation of H_2O ($2\ H_2O \rightarrow O_2 + 4\ H^+ + 4\ e^-$)[5] provides the protons and electrons that can be used to drive a multitude of subsequent reactions, either directly or *via* the formation of H_2. The high thermodynamic and kinetic stability of several of these molecules (e.g., CO_2 and N_2), and the multi-step, multi-electron nature of their transformation places significant demands on catalyst design: catalysts should be stable in a variety of redox-states, be able to efficiently transform a multitude of intermediates *en route* to the final product(s), and at the same time have low activation barriers for each individual step in the reaction sequence. Against this backdrop, it is perhaps not surprising that there is much interest in molecular catalysts for energy applications, since these offer the possibility to tune catalyst properties with great precision via rational molecular design, and can provide detailed insight in the reaction mechanism(s) at play.

The majority of synthetic molecular catalysts that operate *via* elementary steps involving changes in oxidation state are proposed to do so by changing the formal oxidation state of the central metal atom. In contrast, Nature often uses metalloenzymes in which there is an organic redox-active cofactor adjacent or bound to the active site. The role of these redox-active moieties is to accumulate redox equivalents that can subsequently be used by the metalloenzyme to perform challenging multi-electron transformations. Examples of such metalloenzymes include galactose oxidase[6] and cytochrome P450s,[7] which store redox-equivalents in the organic ligand scaffold to ultimately perform 2-electron oxidation of alcohols and aliphatic CH bonds, respectively. Inspired by these enzymatic systems, there is increasing interest in the chemistry of synthetic catalysts with redox-active ligands.[8] The electronic

structure of such complexes, which underpins our understanding of reactivity, is only beginning to be uncovered in recent years. As an example, iron porphyrin complexes that perform electrocatalytic CO_2 reduction at the formal Fe(0) potential have recently been shown to consist of an intermediate-spin Fe(II) center that is anti-ferromagnetically coupled to a 2-electron reduced porphyrin diradical; the reducing equivalents in this catalyst species thus reside on the organic ligand.[9] Moreover, electrocatalytic CO_2 reduction using a porphyrin complex with a redox-innocent Zn(II) ion was recently reported,[10] further highlighting the importance of ligand-based redox-reactions in these systems. Recent studies on azo-containing pincer ligands have shown that also alcohol dehydrogenation can be catalyzed *via* a pathway that involves a reduced azo moiety.[11] Similarly, studies on molecular electrocatalysts for the hydrogen evolution reaction (HER) have identified several systems in which the mechanism does not involve 'traditional' metal-hydride intermediates;[12] instead, the organic ligand is proposed to be involved as the locus of reduction, protonation, or both. Thus, the assembly of 2 protons and 2 electrons as required for H_2 production requires a delicate interplay between the reactivity of the metal center and that of the ligand. Illustrative examples include cobaloximes[13] (Chart 3.1, **A**) and related compounds,[14] for which there has been considerable debate on the intermediates that lead to H_2 formation,[15,16] and nickel diphosphine complexes with a 'pendant' proton-relay site (Chart 3.1, **B**).[17] In addition, hydrogen evolution catalysts are known with 'redox-active' ligands: homogeneous Co dithiolene compounds have been pioneered by Holland and Eisenberg (Chart 3.1, **C**),[18,19,20] and these were recently extended to heterogeneous systems,[21]

Chart 3.1

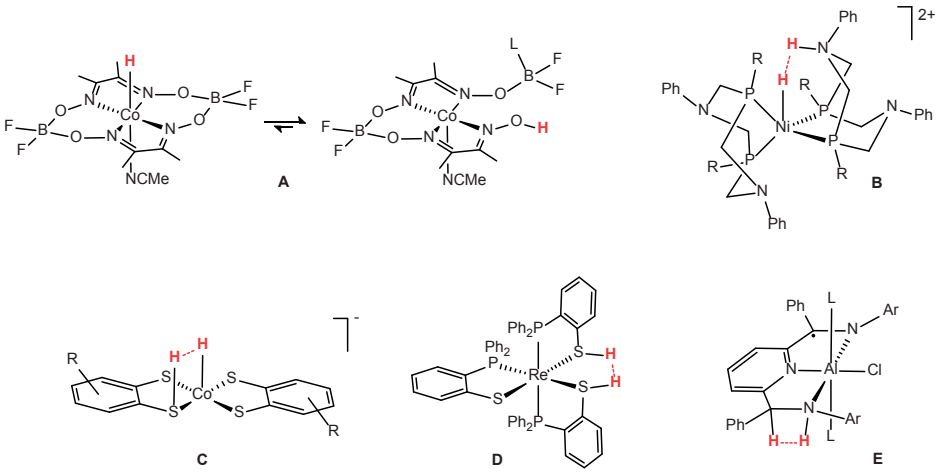

and their mechanism studied computationally.[22] Recent work from Grapperhaus and co-workers identified homogeneous proton reduction catalysts that proceed *via* ligand-centered reactions in which metal-hydride species are not involved (Chart 3.1, **D**),[23] and also nickel porphyrin HER catalysts have been shown to undergo reduction/protonation to lead to an organic hydride as key intermediate that generated by ligand-based [$2e^-/H^+$] reactivity.[24] In addition to catalysts containing transition metal centers, examples have been reported of main group complexes that are active in hydrogen evolution,[25] as illustrated by Berben's aluminum complexes with reduced pyridinediimine ligand (Chart 3.1, **E**).

The mechanistic ambiguities in (electro)catalysis and the new types of reactivity that can result with metal complexes that contain redox-active ligands make these interesting systems for further exploration. Intrigued by work from the Hicks group on formazanate ligands as nitrogen-rich, redox-active analogues of the well-known β-diketiminates,[26] our group has started a research program to explore the coordination chemistry, redox-behavior and reactivity of complexes with formazanate ligands.[27] Although some early reports on related complexes exist,[28,29] it is only recently that interest in this class of ligands has gained momentum. Concurrent with our work, the Gilroy group and others have reported related complexes with formazanate ligands and studied the properties of these compounds[30,31] and materials derived

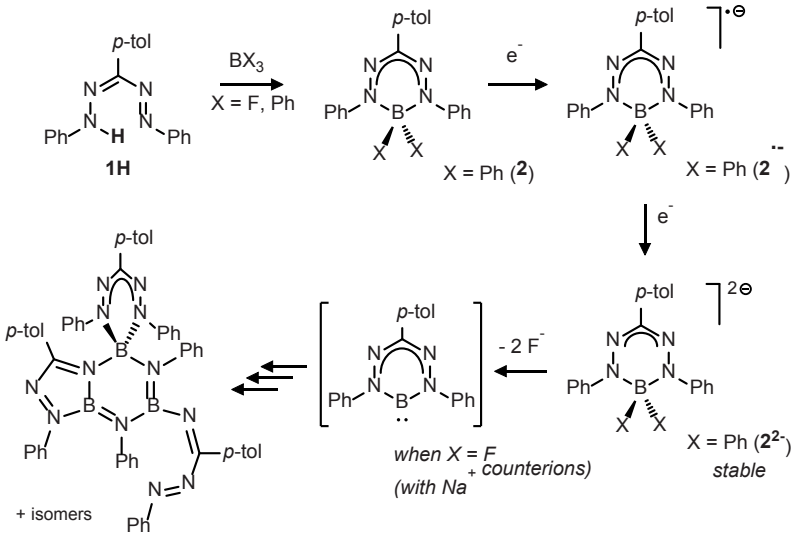

Scheme 3.1 Synthesis of 1- and 2-electron reduced boron formazanate compounds, and their conversion to BN heterocyclic products *via* a *N*-heterocyclic B(I) carbenoid intermediate.

thereof.[32] Previously, we studied ligand-based reductions in formazanate boron compounds,

and showed that both 1- and 2-electron reduced products can be obtained (Scheme 3.1).[33] For the boron difluoride derivative, 2-electron reduction leads to elimination of 2 equiv of F^- and formation of a boron carbenoid intermediate, the fate of which is ultimately a series of B_3N_3 heterocyclic products that incorporate the (formazanate)B fragment (Scheme 3.1).[34]

In this chapter, we present boron complexes with the formazanate ligand L ($LBPh_2$; L = [PhNNC(*p*-tol)NNPh]$^-$, **1**), and explore the nucleophilic reactivity of the corresponding 2-electron reduced complex, $[LBPh_2]^{2-}$ ($\mathbf{2^{2-}}$) with the electrophiles BnBr and H_2O (the synthesis and characterization of **2**, $\mathbf{2^{\cdot-}}$ and $\mathbf{2^{2-}}$ have been presented in chapter 2). The products are group 13 analogues of leucoverdazyls (tetrahydro-1,2,4,5-tetrazines). Our results demonstrate that, starting from neutral $LBPh_2$ (**2**), sequential 'storage' of 2 electrons and an equivalent of electrophile ($E^+ = Bn^+, H^+$) occurs in this main group compound, an overall [$2e^-/E^+$] process that takes place exclusively at the organic ligand. The ability of the products to subsequently undergo homolytic N-H and N-C bond cleavage was investigated by exchange NMR spectroscopy and kinetic experiments.

3.2 Reactivity of 2-electron reduced formazanate boron diphenyl compound with electrophiles

3.2.1 Ligand-centered storage of 2-electron and electrophile ($2e^-/E^+$) in formazanate boron diphenyl compound

The ligand **1H**, its corresponding boron complex $LBPh_2$ (**2**) and the dianion $[LBPh_2]^{2-}$ ($\mathbf{2^{2-}}$) were prepared as reported previously (Scheme 3.1).[33c] Treatment of the 2-electron reduced, dianionic formazanate boron compound $[LBPh_2]^{2-}$ ($\mathbf{2^{2-}}$) with BnBr on NMR scale in THF-d_8 resulted in clean formation of a new compound. The appearance of a set of (broad) diastereotopic protons at δ 3.78 and 3.42 ppm in the ^{1}H NMR spectrum is indicative of a benzyl group attached to an N-atom of the formazanate ligand, and the product is formulated as the ligand-benzylated compound $[^{Bn}LBPh_2]^-$ ($\mathbf{^{Bn}3^-}$, Scheme 3.2). Repeating the reaction on a preparative scale allowed isolation of $\mathbf{^{Bn}3^-}$ (as its sodium salt) in 92 % yield as a waxy green solid upon precipitation with hexane. NMR analysis of isolated $\mathbf{^{Bn}3^-}$ at room temperature in THF-d_8 solution shows fluxional behavior with several resonances being broadened. A variable temperature NMR study (500 MHz, THF-d_8) in the temperature range between -30 and +70 °C shows that the broadening of the diastereotopic benzyl-CH_2 resonances is due to chemical exchange: two sharp doublets are observed at -25 °C (3.79 and 3.38 ppm) that are mutually coupled with $^2J_{HH}$ = 15.3 Hz. At 70 °C, these signals are coalesced and appear as a sharp singlet

at 3.69 ppm. Resonances due to the phenyl groups bound to boron are also exchange-broadened, with two distinct BPh resonances observed at low temperature that coalesce to a single set for the BPh_2 moiety at temperatures > 65 °C. These observations are taken as indication that in the highly congested structure of ^{Bn}**3**$^-$ the rotation around the N-CH_2Ph bond is 'geared' to rotation of the B-Ph moieties. The *para*-H atoms of the inequivalent N-Ph rings in ^{Bn}**3**$^-$ are observed at δ 6.16 and 6.07 ppm, and the former shows additional coupling, the magnitude of which is temperature-dependent. We attribute this feature to through-space interactions with protons of the N-benzyl ring due to their close proximity. The ^{11}B NMR resonance at 1.16 ppm is indicative of a 4-coordinate boron center, supporting the assignment of ^{Bn}**3**$^-$ as a boron diphenyl complex with a benzylated formazanate fragment. The reaction of **2**$^{2-}$ with BnBr is best regarded as a S_N2-type nucleophilic substitution, with the highly charged formazanate ligand in **2**$^{2-}$ acting as the nucleophile.

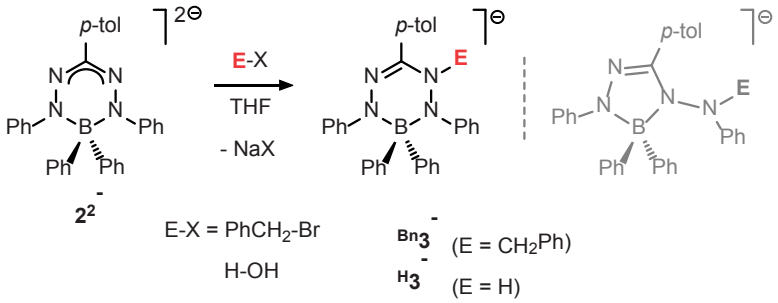

Scheme 3.2 Synthesis of compounds ^{Bn}**3**$^-$ and ^{H}**3**$^-$

Similarly, reaction of **2**$^{2-}$ with an equivalent of H_2O results in clean formation of the corresponding protonated product ^{H}**3**$^-$ with precipitation of NaOH (Scheme 3.2). The diagnostic N-H resonance of ^{H}**3**$^-$ is found at δ 5.04 ppm in the ^{1}H NMR spectrum, while the ligand and BPh_2 groups in ^{H}**3**$^-$ are similar to those in ^{Bn}**3**$^-$ with two upfield N-Ph NMR resonances due to the *p*-H at δ 6.12 and 6.08 ppm. The similarity of the NMR spectral data for ^{H}**3**$^-$ and ^{Bn}**3**$^-$ suggest that they have comparable structures, with the same site of attack in the formazanate ligand for both electrophiles. The compounds are invariably obtained as oily material, but storage of a sample of ^{Bn}**3**$^-$ (as a green oil) on THF/hexane at -30 °C for several days allowed the oil to solidify and form forest-green crystals. Unfortunately, the crystals melt again when taken out of the mother liquor, and we were unable to obtain structural data by X-ray crystallography. Although in principle two structural types can be plausibly formulated for these compounds (six- and five-membered ring isomers, see Scheme 3.2), NMR spectroscopy is most consistent with a six-membered cyclic structure (shown as $^{Bn/H}$**3**$^-$). In particular, two-dimensional NOESY

NMR spectroscopy showed cross-peaks of similar intensity between the N-H resonance and the ortho-H signals of both the p-tolyl and one of the N-Ph rings, as expected for structures $\mathbf{3}^-$. In addition, a comparison of empirical and DFT calculated NMR chemical shifts is most consistent with six-membered chelate rings (see Supporting Information for details). Six-membered ring carbon-based analogues of $\mathbf{3}^-$ (leucoverdazyls) are well-established in the literature, and the reactivity of $^{Bn/H}\mathbf{3}^-$ (vide infra) is similar to that in the organic analogues.[35] Finally, the exchange of sodium counter cation in [$^{Bn}\mathbf{3}$][**Na**] by the NBu_4 leads to formation of [$^{Bn}\mathbf{3}$][$\mathbf{NBu_4}$], which is crystalline and does not melt even at room temperature for several days, allows us to determine its structure by X-ray crystallography. The molecular structure of [$^{Bn}\mathbf{3}$][$\mathbf{NBu_4}$] reveals that the benzyl group is attached to one of the internal N-atoms, and maintains the 6-membered chelate ring structure of its dianionic precursor (for the detailed analysis of the crystallographic data of [$^{Bn}\mathbf{3}$][$\mathbf{NBu_4}$] please see chapter 5). On the basis of these considerations, we propose the compounds $^{Bn/H}\mathbf{3}^-$ to have the structures shown in Scheme 3.2. Related charge-neutral boron hydride compounds were prepared by thermolysis of (formazanate)BH_2 compounds. In these systems, intramolecular transfer of a hydride from the BH moiety onto the formazanate ligand occurs at ca. 100 °C, which also formally involves a [$2e^-/H^+$] modification of the ligand, but this is accompanied by N-N bond cleavage as the result of a second hydride being transferred.[36] The current approach of sequential 2-electron reduction followed by external electrophile addition leads to clean formation of 'borataleucoverdazyls', a class of compounds that has not been prepared previously.

The UV/Vis spectra of compounds $^{H}\mathbf{3}^-$ and $^{Bn}\mathbf{3}^-$ in THF are similar and show absorption maxima at 400 and 395 nm, respectively, presumably due to a $\pi\rightarrow\pi^*$ transition in the (localized) N=C bond (Figure S3.2). These bands are shifted to higher energies in comparison to the intense $\pi\rightarrow\pi^*$ transition band in compounds with fully delocalized formazanate ligands (e.g., λ_{max} = 500 nm in **2**), but in the same range as that found in complexes with the same oxidation state of the ligand (L^{3-}), such as the precursor $\mathbf{2}^{2-}$ (λ_{max} = 389 nm).[33c]

3.2.2 Investigation of hydrogen evolution from $^{H}\mathbf{3}^-$

In the context of proton reduction chemistry, it was of interest to evaluate the further reactivity of these compounds. The anionic boron compounds $^{Bn/H}\mathbf{3}^-$ are unreactive towards an additional equivalent of electrophile (BnBr or H_2O), but do react with strong acids such as *p*-toluenesulfonic acid. The NMR spectra of these reactions, however, show a complex mixture, and in no case could the formation of H_2 (or BnH) be ascertained. The lack of controlled further

reactivity of $^{Bn/H}\mathbf{3}^-$ (other than decomposition to unidentified products when reacted with strong acid) might indicate that these anionic compounds are not sufficiently basic (nucleophilic) to react with mild electrophiles. Although these preliminary data suggest that in the present system the accumulation of the [$2e^-/2H^+$] equivalents required for proton reduction is not feasible, we anticipate that changes in ligand substitution pattern and/or the use of acids of intermediate pK_a might solve these problems. It is important to note that ligand-centered reactions that accumulate two electrons and a proton ([$2e^-/H^+$]) were recently shown to generate an organic 'hydride equivalent' in the case of a nickel 'hangman' porphyrin that is able to release H_2 following a second protonation step.[24] In this system, the sequence of reduction/protonation events (and thus the mechanism of H_2 evolution catalysis) was shown to be highly dependent on acid strength. Our results demonstrate that a similar accumulation of [$2e^-/H^+$] can take place in the boron complex **2**, but the reactivity of the resulting organic (ligand) 'hydride' needs further exploration.

3.2.3 Exploration of N-H and N-C bonds cleavage in $^{H}\mathbf{3}^-$ and $^{Bn}\mathbf{3}^-$

3.2.3.1 Investigation of N-H bond cleavage in $^{H}\mathbf{3}^-$ by 2D EXSY NMR spectroscopy

Given the similarity of the anionic compounds $^{Bn/H}\mathbf{3}^-$ to neutral leucoverdazyls (1,2,3,4-tetrahydro-1,2,4,5-tetrazines), we became interested in the cleavage of the N-H and N-C bond in these systems. Hicks and co-workers recently described that coordination to a Ru center weakens the N-C bond in an *N*-benzyl tetrazine *via* metal-ligand non-innocence, and leads to homolysis that is ca. 40 times faster than without metal bound.[37] The influence of main group or transition metal elements incorporated *into* these heterocyclic structures has not been studied before, but homolytic cleavage is expected to generate the radical anions $\mathbf{2}^{\bullet-}$ which contain ligand-based radicals and are relatively stable due to delocalization of the unpaired electron over all 4 nitrogen atoms (Figure S3.11).[33c,35b] For the 'borataleucoverdazyl' $^{H}\mathbf{3}^-$, its lack of symmetry (C_1) results in inequivalent N-Ph groups, and 2D EXSY NMR spectroscopy in THF-d_8 solution shows chemical exchange cross-peaks between the well-separated *ortho*-H resonances of these rings, which is the result of net H-atom transfer between the two 'internal' nitrogens in the ligand backbone. The mechanism of H-atom transfer can either occur *via* a dissociative mechanism (N-H bond homolysis) or intramolecularly *via* a bimolecular (associative) pathway. To probe the mechanism of H-atom transfer, the exchange kinetics were measured by 2D EXSY NMR spectroscopy in the temperature range 10 – 65 °C. Subsequent

Eyring analysis afforded the activation parameters as $\Delta H^{\ddagger} = 44.2 \pm 0.9$ kJ·mol^{-1} and $\Delta S^{\ddagger} = -93 \pm 3$ J·mol^{-1}·K^{-1} (see Supporting Information for details). The large, negative activation entropy is in agreement with a bimolecular mechanism, and the activation enthalpy is too low for (homolytic) N-H bond dissociation as the rate-determining step. An estimation of the N-H bond dissociation energy using DFT calculations (via geometry optimizations at increasing N-H distances) reveals a value of ca. 275 kJ·mol^{-1}, in agreement with the experimental values for leucoverdazyls (281-307 kJ·mol^{-1}).[38] These arguments support a (symmetrical) exchange pathway *via* the bimolecular mechanism shown in Scheme 3.3.

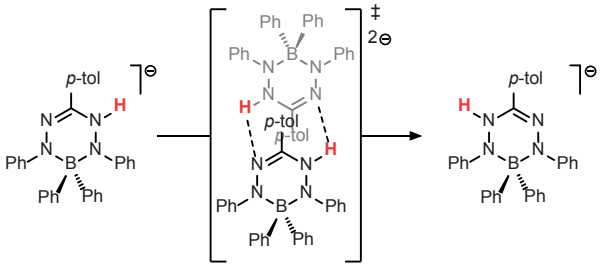

Scheme 3.3 Proposed bimolecular (associative) mechanism for the exchange process in ^{H}**3**$^{-}$

3.2.3.2 Investigation of N-H bond Cleavage in ^{H}3^{-} by following the kinetics of H-atom transfer to TEMPO

The reaction of ^{H}**3**$^{-}$ with TEMPO in THF is fast and generates **2**$^{\bullet-}$ according to EPR spectroscopy by comparison to an authentic sample (Figure S3.1). Despite the presence of paramagnetic species, the ^{1}H NMR spectra show relatively sharp resonances for ^{H}**3**$^{-}$ and TEMPO-H, and complete (> 95%) consumption of the starting material for a 1:1 mixture indicates that the N-H bond in ^{H}**3**$^{-}$ is weaker than in TEMPO-H, for which a bond dissociation free energy of 270-280 kJ·mol^{-1} in organic solvents has been reported.[39]

3.2.3.3 Investigation of N-C(Bn) bond cleavage in ^{Bn}3^{-} by following the kinetics of benzyl transfer to TEMPO

In contrast to ^{H}**3**$^{-}$, the benzyl analogue ^{Bn}**3**$^{-}$ does not show 2D EXSY NMR cross-peaks even at elevated temperature (75 °C). This likely is due to a change in mechanism, with (dissociative)

homolytic cleavage of the N-C bond now operative. To obtain insight in the N-C(Bn) bond dissociation energy, the kinetics of benzyl transfer from ^{Bn}**3**$^{-}$ to TEMPO were measured in the temperature range between 55 – 85 °C (Scheme 3.4). To effectively trap the Bn· radical formed, kinetic experiments were carried out in the presence of 20 equiv. of TEMPO. Monitoring the reaction at regular time intervals by ^{1}H NMR spectroscopy showed clean exponential decay of the starting material and concomitant appearance of TEMPO-Bn. Eyring analysis afforded the activation parameters as $\Delta H^{\ddagger} = 121 \pm 5$ kJ·mol^{-1} and $\Delta S^{\ddagger} = 77 \pm 14$ J·mol^{-1}·K^{-1} (see Supporting Information for details). Under similar conditions, transfer of the 4-fluorobenzyl group in $^{F\text{-}Bn}$**3**$^{-}$ to TEMPO was evaluated, which was shown to have activation parameters of $\Delta H^{\ddagger} = 107 \pm 3$ kJ·mol^{-1} and $\Delta S^{\ddagger} = 36 \pm 9$ J·mol^{-1}·K^{-1}. In agreement with rate-determining N-C(Bn) bond homolysis, the activation entropy is large and positive, and $\Delta H^{\ddagger}$ can be taken as an approximation of the N-C bond dissociation enthalpy.[37,40] The $\Delta H^{\ddagger}$ values of 121 ± 5 and 107 ± 7 kJ·mol^{-1} for ^{Bn}**3**$^{-}$ and $^{F\text{-}Bn}$**3**$^{-}$, respectively, are somewhat smaller than that in pure carbon-based N-alkyl substituted benzyl tetrazines,[37,41] and fall in the lower range of C-O BDEs in the well-studied alkoxyamines[40,42] or Ti-O BDEs in titanocene(IV) complexes derived from nitroxyl radicals.[43]

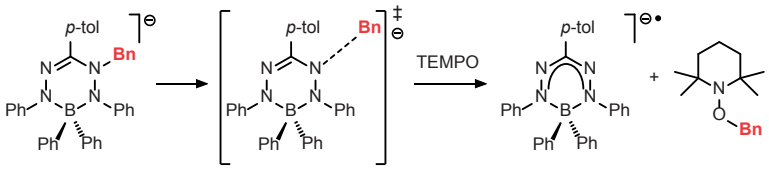

Scheme 3.4 Kinetics of benzyl transfer from ^{Bn}**3**$^{-}$ to TEMPO

3.3 Conclusions

In conclusion, this work shows that the ligand in formazanate boron complexes is reactive and can be used to accumulate [2e^{-}/E^{+}] equivalents (E^{+} = Bn^{+}, H^{+}), a step that has precedent in non-traditional hydrogen evolution catalysts (i.e., those not going through metal-hydride intermediates; E^{+} = H^{+}).[24] Although preliminary attempts to elicit 'organohydride' reactivity in ^{H}**3**$^{-}$ by protonation, a reaction relevant to hydrogen evolution, were not successful, the compounds $^{Bn/H}$**3**$^{-}$ are shown to have weak N-H/N-C bonds that are readily cleaved homolytically. Our results complement Hicks' observation that N-C bond homolysis in coordinated leucoverdazyls may be controlled by metal-ligand covalency and consequent spin-delocalization onto the metal center. The incorporation of an element other than carbon (here, boron) in the six-membered ring of leucoverdazyls similarly allows modulation of homolytic

N-C and N-H bond cleavage energies. The weak N-C and N-H bonds in these systems is the result of the stability of the resulting boron formazanate radical ('borataverdazyl') species. Having established the first synthesis and characterization of 'borataleucoverdazyls', we are currently exploring ligand substituent effects on the reactivity of these compounds. In general, we anticipate that the ability to influence basicity, radical stability and N-H/N-C bond strength of compounds containing the formazanate ligand, either *via* substituent effects or by incorporation of different central elements (main group or transition metal) can be used to modulate reactivity and steer it away from the observed radical reactions (H·/Bn· transfer) towards multi-electron reactions (e.g., [$2e^-/2H^+$]). These reactions are of fundamental importance, for example in electrocatalytic hydrogen evolution, and we are actively working towards applying our systems in this area.

3.4 Experimental section

3.4.1 General considerations

All manipulations were carried out under nitrogen or argon atmosphere using standard glovebox, Schlenk, and vacuum-line techniques. Toluene and hexane (Aldrich, anhydrous, 99.8%) were passed over columns of Al_2O_3 (Fluka), BASF R3-11-supported Cu oxygen scavenger, and molecular sieves (Aldrich, 4 Å). THF (Aldrich, anhydrous, 99.8%) was dried by percolation over columns of Al_2O_3 (Fluka). The compounds $^{H}\mathbf{3}^-$, $^{Bn}\mathbf{3}^-$ and $^{F\text{-}Bn}\mathbf{3}^-$ are highly air-sensitive, and the solvents (THF and hexane) used for their preparation and characterization were additionally dried on Na/K alloy and subsequently vacuum transferred and stored under nitrogen. All solvents were degassed prior to use and stored under nitrogen. d_8-THF (Sigma-Aldrich) was vacuum transferred from Na/K alloy and stored under nitrogen. The compound $\mathbf{2}^{2-}$ (as its disodium salt, $[(PhNNC(p\text{-}tol)NNPh)BPh_2][Na_2(THF)_6]$) was synthesized according to a published procedure.[33c] NMR spectra were recorded on Varian Mercury 400 or Inova 500 or Bruker 600 spectrometers. The ^1H and ^{13}C NMR spectra were referenced internally using the residual solvent resonances and reported in ppm relative to TMS (0 ppm); *J* is reported in Hz. Assignments of NMR resonances was aided by COSY, NOESY, HSQC and HMBC experiments using standard pulse sequences. UV-Vis spectra were recorded in THF solution (~ 10^{-3} M) in a quartz cuvette using an AVANTES AvaSpec-2048. Samples for elemental analyses were sent to Kolbe Microanalytical Laboratory (Mülheim an der Ruhr, Germany). However, despite our best efforts, no satisfactory analysis data could be obtained for these compounds, which is likely due to their highly air-sensitive nature and/or to the fact that these compounds are oily and therefore still contain residual solvent and/or (unknown) impurities. It should be noted, however, that NMR spectroscopy indicates that compounds $^{H/Bn}\mathbf{3}^-$ are formed cleanly (>90% by integration relative to an internal standard).

3.4.2 Compounds synthesis and characterization

Synthesis of $[^{H}LBPh_2]Na(THF)_2$ ($^{H}\mathbf{3}^-$). Compound $\mathbf{2}^{2-}$ (400 mg, 0.598 mmol) was dissolved in 2 ml of THF in a Schlenk tube inside the glove box. To this was added 1 equiv of H_2O (as a dilute solution in THF), which caused the color to change from orange to purple-red. After stirring the mixture for 1 hour, all the volatiles were removed under reduced pressure and the crude product was washed with hexane (3 x 2ml). Subsequently, drying under vacuum gave compound $^{H}\mathbf{3}^-$ as an oily green material (339 mg, 0.524 mmol, 87 %). ^1H NMR (500 MHz, THF-d_8, -5 °C) δ 7.79 (d, *J* = 8.0 Hz, 2H, *p*-tol *o*-H), 7.39 (d, *J* = 7.1 Hz, 4H, BPh *o*-H), 7.01 (d, *J* = 8.0 Hz, 2H, *p*-tol *m*-H), 6.97 (d, *J* = 7.9 Hz, 2H, N(2)Ph *o*-H), 6.91 (t, *J* = 7.1 Hz, 4H,

BPh *m*-H), 6.85 (t, *J* = 7.1 Hz, 2H, BPh *p*-H), 6.67 – 6.52 (overlapped, 6H, N(1)Ph (*o*+*m*)-H and N(2)Ph *m*-H), 6.12 (t, *J* = 7.0 Hz, 1H, N(2)Ph *p*-H), 6.08 (t, *J* = 6.8 Hz, 1H, N(1)Ph *p*-H), 5.04 (s, 1H, NCN-H), 3.62 (m, 10H, THF), 2.28 (s, 3H, *p*-tol CH_3), 1.78 (m, 10H, THF). ^{11}B NMR (128.0 MHz, THF-d_8, 25 °C) δ 0.4 (s). ^{13}C NMR (125 MHz, THF-d_8, -5 °C) δ 156.39 (BPh *ipso*-C), 155.14 (N(1)Ph *ipso*-C), 154.55 (N(2)Ph *ipso*-C), 138.48 (N**C**N), 136.20 (*p*-tol **C**-NCN), 135.88 (BPh *o*-CH), 135.62 (*p*-tol **C**-CH_3), 128.75 (*p*-tol *m*-CH), 127.40 (N(2)Ph *m*-CH), 126.86 (BPh *m*-CH), 126.78 (N(1)Ph *o*-CH), 125.47 (*p*-tol *o*-CH), 124.33 (BPh *p*-CH), 118.94 (N(2)Ph *o*-CH), 117.35 (N(1)Ph *m*-CH), 113.93 (N(2)Ph *p*-CH), 113.31 (N(1)Ph *p*-CH), 68.30 (THF), 26.44 (THF), 21.41 (*p*-tol CH_3).

Synthesis of [^{Bn}LBPh$_2$]Na(THF)$_2$ (^{Bn}3$^-$). Compound **2**$^{2-}$ (400 mg, 0.498 mmol) was dissolved in 2 ml of THF in a Schlenk tube inside the glove box. To this was added 1 equiv of benzyl bromide, which caused the color to change from orange to purple-red. After stirring the mixture for 1 hour, all the volatiles were removed under reduced pressure and the crude product was washed with hexane (3 x 2ml). Subsequently, drying under vacuum gave compound ^{Bn}**3**$^-$ as an oily green material (292 mg, 0.450 mmol, 92 %). ^{1}H NMR (600 MHz, THF-d_8, 10 °C) δ 7.83 (d, J = 8.1 Hz, 2H, p-tol *o*-H), 7.69 (d, J = 6.9 Hz, 2H, B(1)Ph *o*-H), 7.09 (t, J = 7.0 Hz, 2H, B(1)Ph *m*-H), 7.05 – 6.98 (overlapped, 6H, (benzyl)Ph *o*-H, B(2)Ph *o*-H and p-tol *m*-H), 6.97 (t, J = 7.0 Hz, 1H, B(1)Ph *p*-H), 6.94 (d, J = 6.4 Hz, 2H, N(1)Ph *o*-H), 6.87 – 6.79 (m, 3H, (benzyl)Ph (*m*+*p*)-H), 6.57-6.53 (overlapped, 5H, N(1)Ph *m*-H and B(2)Ph (*m*+*p*)-H), 6.47-6.45 (m, 4H, N(2)Ph (*o*+*m*)-H), 6.17 – 6.14 (m, 1H, N(2)Ph *p*-H), 6.07 (t, J = 7.0 Hz, 1H, N(1)Ph *p*-H), 3.78 (d, J = 15.3 Hz, 1H, benzyl-CH_2), 3.62 (m, 8H, THF), 3.42 (d, J = 15.3 Hz, 1H, benzyl-CH_2), 2.28 (s, 3H, *p*-tol CH_3), 1.78 (m, 8H, THF). ^{11}B NMR (128.3 MHz, THF-d_8, 25 °C) δ 1.16 (s). ^{13}C NMR (150 MHz, THF-d_8, 10°C) δ 158.66 (N(2)Ph *ipso*-C), 155.48 (B(1,2)Ph *ipso*-C), 154.07 (N(1)Ph *ipso*-C), 142.34 (NCN), 141.66 ((benzyl)Ph ipso-C)), 137.67 (NCN-*p*-tol *ipso*-C), 137.17 (B(1)Ph *o*-CH), 137.08 (B(2)Ph *o*-CH), 135.25 (*p*-tol-CH_3 *ipso*-C), 129.62 ((benzyl)Ph *o*-CH), 128.77 (*p*-tol *m*-CH), 127.41 (*p*-tol *o*-CH), 127.34 ((benzyl)Ph *p*-CH), 126.59 (B(2)Ph *m*-CH), 126.33 (B(1)Ph *m*-CH), 126.14 (N(2)Ph *o*-CH), 125.69 (B(2)Ph *p*-CH), 125.64 ((benzyl)Ph *m*-CH), 124.03 (B(1)Ph *p*-CH), 123.77 (N(2)Ph *p*-CH), 123.40 (N(1)Ph *m*-CH), 118.56 (N(1) Ph *o*-CH), 116.37 (N(2)Ph *p*-CH), 113.78 (N(1)Ph *p*-CH), 68.29 (THF), 26.45 (THF), 21.37 (*p*-tol CH_3).

Synthesis of [$^{F\text{-}Bn}$LBPh$_2$]Na(THF)$_2$ ($^{F\text{-}Bn}$3$^-$). Compound **2**$^{2-}$ (100 mg, 0.12 mmol) was dissolved in 1 ml of THF in a Schlenk tube inside the glove box. To this was added 1 equiv of

4-fluorobenzyl bromide, which caused the color to change from orange to purple-red. After stirring the mixture for 1 hour, all the volatiles were removed under reduced pressure and the crude product was washed with hexane (3 x 2ml). Subsequently, drying under vacuum gave compound $^{F\text{-}Bn}$**3**$^{-}$ as an oily purple-red material (72 mg, 0.095 mmol, 79 %). ^{1}H NMR (400 MHz, THF-d_8, 25 °C) δ 7.81 (d, J = 8.1 Hz, 2H, *p*-tol *o*-H), 7.69 (bs, 2H, BPh *o*-H), 7.10 (bs, 3H, BPh (*m*+*p*)-H), 7.02 (overlapped, 4H, BPh *o*-H and p-tol *m*-H), 7.00 – 6.96 (m, 2H, (benzyl)Ph *o*-H), 6.95 (d, J = 8.1 Hz, 2H, N(1)Ph *o*-H), 6.55 (overlapped, 7H, (benzyl)Ph *m*-H, N(1)Ph *m*-H and BPh (*m*+*p*)-H), 6.47-6.45 (m, 4H, N(2)Ph (*o*+*m*)-H), 6.16 (m, 1H, N(2)Ph *p*-H), 6.07 (t, J = 7.1 Hz, 1H, N(1)Ph *p*-H), 3.75 (d, J = 15.0 Hz, 1H, benzyl-CH_2), 3.39 (d, J = 15.0 Hz, 1H, benzyl-CH_2), 2.29 (s, 3H, *p*-tol CH_3). ^{19}F NMR (376 MHz, THF-d_8, 25 °C) δ -118.45 (m, benzyl *p*-F).

3.5 Supplementary information

3.5.1 EPR spectral data

A solution of ^{H}**3**$^{-}$ or ^{Bn}**3**$^{-}$ in THF was reacted with 1 equiv of TEMPO at room temperature for about 1 h (for ^{H}**3**$^{-}$) or at 60 ˚C for about 12 hrs (for ^{Bn}**3**$^{-}$). Then EPR spectra of the reaction mixtures were taken. The EPR spectra indicated formation of the radical anion **[LBPh$_2$]$^{\bullet-}$** (**2**$^{\bullet-}$) by comparison to an authentic sample.

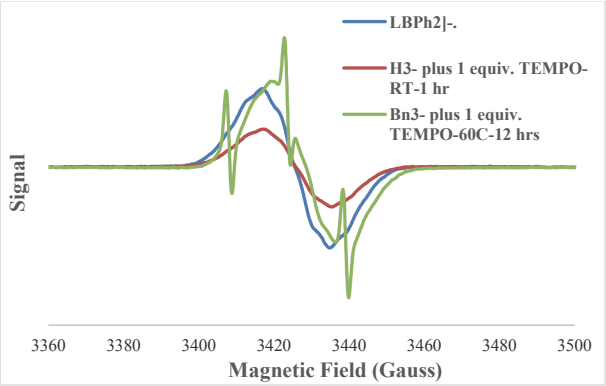

Figure S3.1 EPR data of authentic sample of **2**$^{\bullet-}$ (**blue**); reaction mixture of ^{H}**3**$^{-}$ with 1 equiv. TEMPO at room temperature after 1 hr (**red**); reaction mixture of ^{Bn}**3**$^{-}$ with 1 equiv. TEMPO at 60 ˚C after 12 hrs (**green**) in THF solution. The spectrum in green indicates some left-over TEMPO, likely the result of a slight excess of TEMPO used.

3.5.2 UV-Vis spectral data

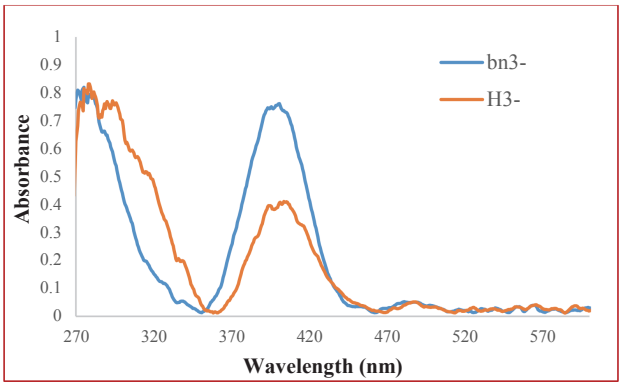

Figure S3.2 UV-Vis absorption spectra of ^{H}**3**$^{-}$ and ^{Bn}**3**$^{-}$ in THF solution

3.5.3 2D EXSY NMR studies

A solution of compound ^{H}**3**$^{-}$ in THF-d_8 was prepared in a J. Young's NMR tube and inserted into the probe of a 500 MHz Varian INOVA NMR spectrometer. EXSY spectra were acquired using a standard NOESY pulse sequence. In the direct time domain the spectral width was set to 6633 Hz (ca. 0 – 15 ppm) with 1194 complex points detected, while in the second time domain a spectral width of 700 Hz was selected around the area of interest (ca. 6.5 – 7.1 ppm). For each experiment, a total of 64 increments was collected to give a resolution of 11 Hz (0.02 ppm) in the second domain. The total experiment time (4 scans per increment, 1 s relaxation delay) for each experiment was ca. 19 min. Data were collected at a series of temperatures between 10 and 65 °C, and at each temperature at least 3 mixing times were chosen such that the ratio of the cross/diagonal peak integration varied between ca. 0.1 – 0.9. This allowed fitting of the exchange build-up curves via equation (1).[44]

$$\frac{I_x}{I_d} = \frac{1-e^{-2kt_{mix}}}{1+e^{-2kt_{mix}}} \qquad with \qquad k = \frac{k_B T}{h} e^{-\frac{\Delta H^{\ddagger} - T\Delta S^{\ddagger}}{RT}} \qquad \text{… equation 1}$$

Initially, attempts to determine peak volumes were carried out using Gaussian fitting with Sparky.[45] The closely spaced, overlapping nature of the resonances resulted in poor fits. Also, determination of peak volumes using sum over ellipse methods did not result in reliable values: the cross peak volumes showed unrealistically large differences. Ultimately, the 2D data were phase-corrected in MestreNova 11 after which a 1D slice was extracted from the 2D data along

F2 at 6.955 ppm (the resonance frequency of one of the exchanging Ph *p*-H signals). Especially at higher temperatures and/or mixing times, the cross-peak showed significant tailing likely due to dipolar coupling effects with neighboring sites (spin diffusion). The 1D traces were integrated carefully, in order to minimize contamination due to this tailing (see Figure S3.3 for an example of a 2D spectrum and 1D trace). Although we acknowledge that this is somewhat arbitrary (peak deconvolution techniques were unsuccessful) and thus results in a relatively large error in the integral values, it provides values that are internally consistent based on the fitting to equation 1.

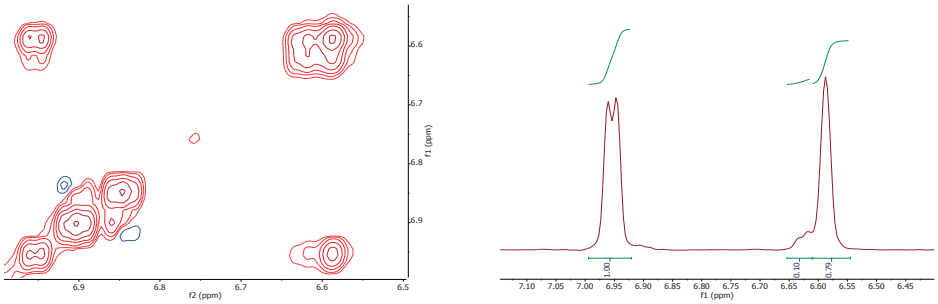

Figure S3.3 2D spectrum ^{H}**3**$^{-}$ at 30 °C for 0.35 s mixing time (left) and it's 1D trace (right)

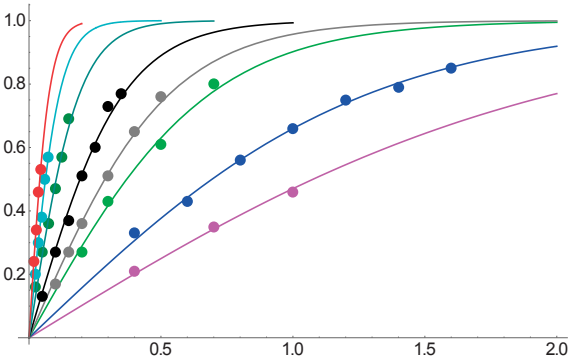

The cross-peak / diagonal peak ratios at each temperature and mixing time were imported into Mathematica 10.3,[46] and a non-linear fit of the data against equation 1 was carried out. The resulting rate constants (*k*) were used to obtain the activation parameters $\Delta H^{\ddagger}$ and $\Delta S^{\ddagger}$ via an Eyring analysis (see Figure S3.4 for both linear and non-linear regression).

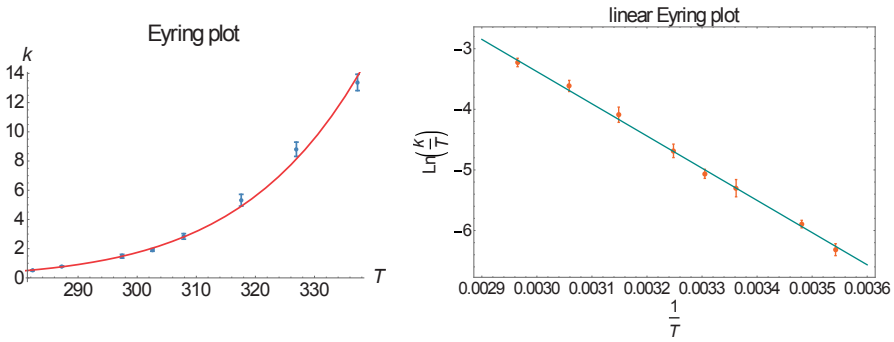

Figure S3.4 Eyring analysis for chemical exchange in ^{H}**3**$^{-}$; $\Delta H^{\ddagger}$ = 44.2 ± 0.9 kJ·mol^{-1} and $\Delta S^{\ddagger}$ = -93 ± 3 J·mol^{-1}·K^{-1}

3.5.4 Analysis of reaction kinetics $^{(F)Bn}$**3**$^{-}$ + TEMPO

A solution of ^{Bn}**3**$^{-}$ or $^{F\text{-}Bn}$**3**$^{-}$ in THF-d_8 was prepared in a J. Young's NMR tube and a few crystals of bibenzyl were added as internal standard. Subsequently, 20 equiv of TEMPO were added to efficiently trap the benzyl radical generated upon thermolysis. The tube was taken out from the glovebox and inserted into the probe of the NMR spectrometer, which was heated to the desired reaction temperature. The NMR probe was tuned and shimmed before insertion of the sample using another NMR tube with the same amount of THF-d_8 at that temperature. After the sample was inserted, an acquisition array was started that was set up to collect spectra at regular time intervals throughout the course of the reaction (see Figure S3.5 and S3.6 for examples of a few traces of the reaction of ^{Bn}**3**$^{-}$ with TEMPO (20 equiv) and for reaction of $^{F\text{-}Bn}$**3**$^{-}$ with TEMPO (20 equiv), respectively). Integration of the TEMPO-Bn resonance (δ 4.82 ppm in the ^{1}H NMR spectrum) or TEMPO-4F-Bn resonance (δ -115.88 ppm in the ^{19}F NMR spectrum) relative to the internal standard (bibenzyl for ^{Bn}**3**$^{-}$ and 2-fluoro-biphenyl for $^{F\text{-}Bn}$**3**$^{-}$) allowed analysis of the rate constant at each temperature by non-linear curve fitting (a+b(1-Exp[-*k*t]) in Mathematica 10.3.[46]

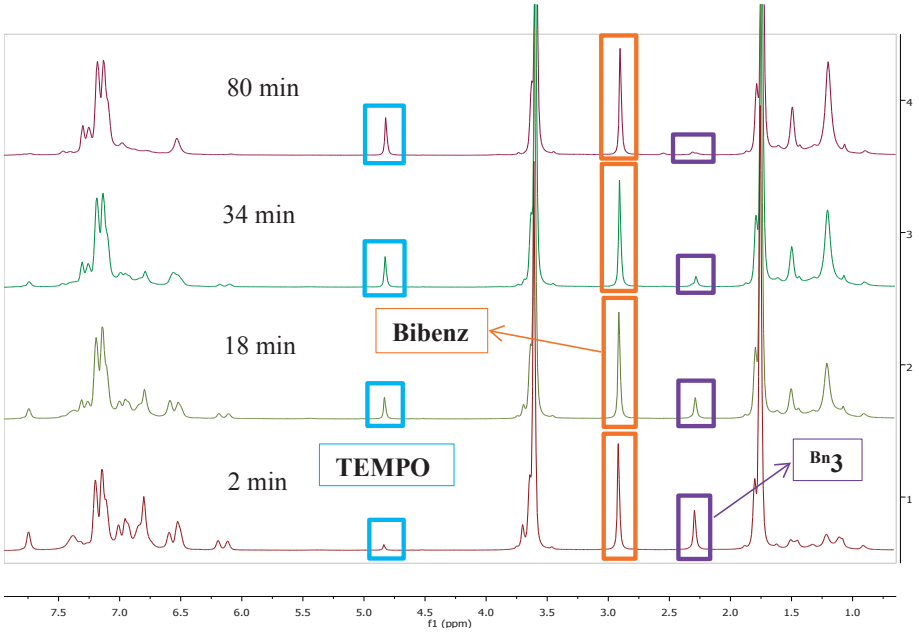

Figure S3.5 Selected ^{1}H-NMR spectra from the 75˚C kinetics array for reaction of ^{Bn}**3**$^{-}$ with TEMPO (20 equiv) in THF-d_8

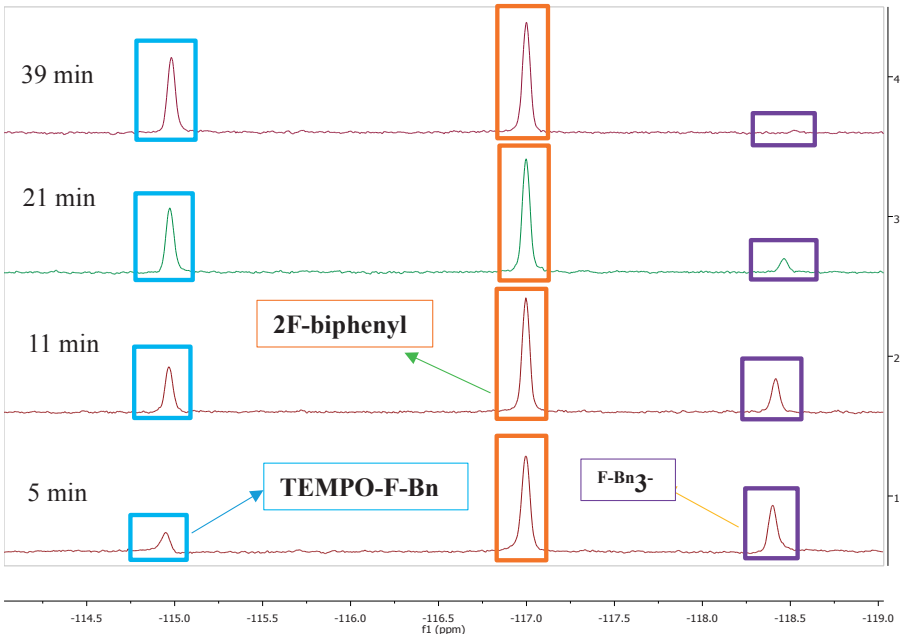

Figure S3.6 Selected ^{19}F-NMR spectra from the 65 ˚C kinetics array for reaction of $^{F\text{-}Bn}$**3**$^{-}$ with TEMPO (20 equiv) in THF-d_8

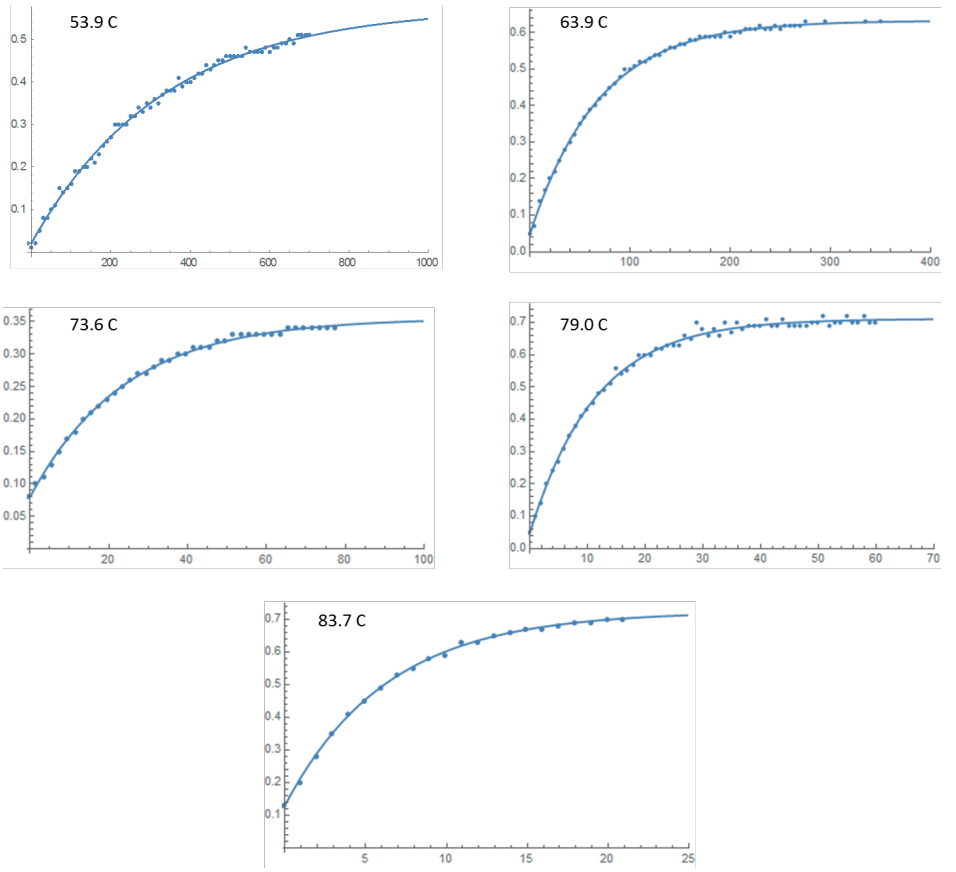

Figure S3.7 Kinetic traces for reaction of ^{Bn}**3**$^{-}$ with TEMPO (20 equiv) in THF-d_8

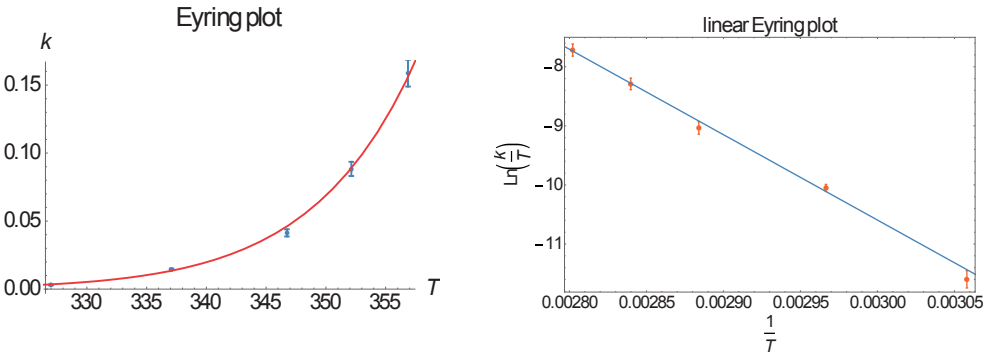

Figure S3.8 Eyring analysis for ^{Bn}**3**$^{-}$; $\Delta H^{\ddagger}$ = 121 ± 5 kJ·mol^{-1} and $\Delta S^{\ddagger}$ = 77 ± 14 J·mol^{-1}·K^{-1}

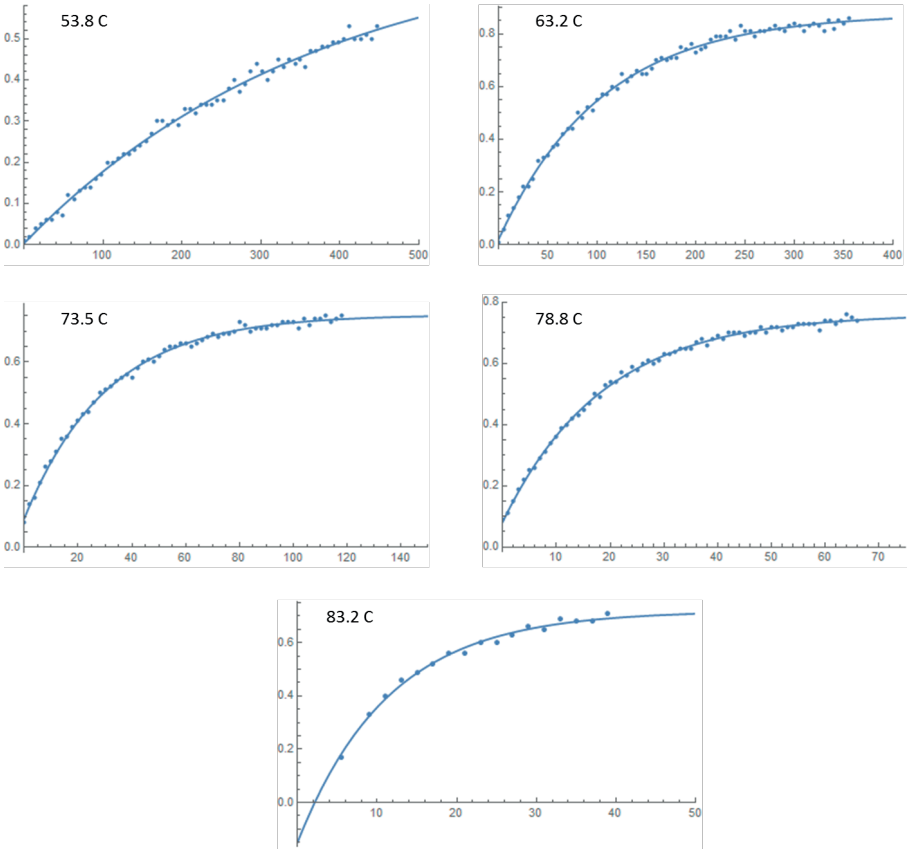

Figure S3.9 Kinetic traces for reaction of $^{\text{F-Bn}}\mathbf{3}^-$ with TEMPO (20 equiv) in THF-d_8

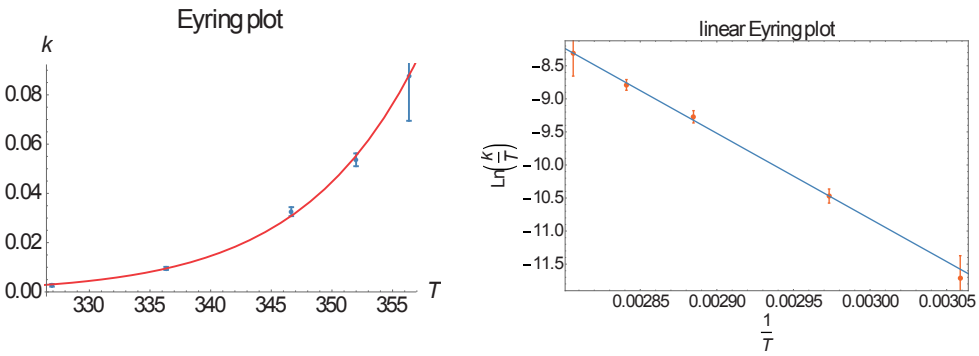

Figure S3.10 Eyring analysis for $^{\text{F-Bn}}\mathbf{3}^-$; $\Delta H^{\ddagger} = 107 \pm 3$ kJ·mol^{-1} and $\Delta S^{\ddagger} = 36 \pm 9$ J·mol^{-1}·K^{-1}

3.5.5 Computational studies

Calculations were performed with the Gaussian09 program[47] using density functional theory (DFT) in the gas phase. The geometry optimization of the radical anion $\mathbf{2}^{-}$ was done using the B3LYP exchange-correlation functional with the 6-311+G(d,p) basis set according to our previously published results.[33c] The geometries of the anions $\mathbf{2}^{2-}$ and $^{\mathbf{H}}\mathbf{3}^{-}$ (without counter cations) were fully optimized using the B3LYP exchange-correlation functional with the 6-311+G(d,p) basis set. As starting point for the optimization of $\mathbf{2}^{2-}$ the crystallographic coordinates were chosen, while those of $^{\mathbf{H}}\mathbf{3}^{-}$ were generated from the crystallographic coordinates of $\mathbf{2}^{2-}$ and adding an additional hydrogen substituent to the appropriate N-atom. The starting point for the geometry optimization of the five-membered chelate ring complex were generated by drawing a reasonable guess geometry in GaussView.[48] Optimizations were performed without (symmetry) constraints, and the resulting structures were confirmed to be minima on the potential energy surface by frequency calculations (number of imaginary frequencies = 0). Calculations of NMR chemical shifts were carried out by single point DFT (B3LYP) calculations on the optimized geometries using the Gauge-Independent Atomic Orbital (GIAO) method implemented in Gaussian09, using a 6-311+G(2d,p) basis set and incorporating THF solvation via the SMD method of Truhlar and co-workers.[49] For both $\mathbf{2}^{2-}$ and $^{\mathbf{H}}\mathbf{3}^{-}$, the 5-membered ring isomers are lowest in energy (ΔG = -3.1 kcal/mol for $\mathbf{2}^{2-}$ and -9.5 kcal/mol for $^{\mathbf{H}}\mathbf{3}^{-}$). In the case of $\mathbf{2}^{2-}$, this is clearly inconsistent with experiment.[33c] We attribute this discrepancy to binding of the cation(s) and/or solvation effects, which can have a significant effect on the relative stabilities of the isomers. The inclusion of the Na^{+} counteraction (and associated THF molecules) was not attempted due to the computational demands of this approach. To obtain further insight in the structure of $^{\mathbf{H}}\mathbf{3}^{-}$, we calculated the NMR spectra of both isomers in THF using the optimized geometries from gas phase calculations. Although these calculations predict very similar ^{1}H NMR shifts for the N-H moiety in both isomers (δ 4.84 and 4.85 ppm), their computed ^{13}C NMR spectra are quite different. In particular, the central C-atom of the ligand backbone has predicted chemical shifts of 162.2 and 144.9 ppm for the five- and six-membered ring isomers, respectively, of which the latter is in good agreement with that measured experimentally (δ 138.5 ppm). Selected experimental and calculated NMR shifts are given in Table S3.1.

Table S3.1 Comparison of experimental and DFT-calculated NMR chemical shifts for diagnostic resonances in isomers of $\mathbf{2}^{2-}$ (top) and $^{\mathbf{H}}\mathbf{3}^{-}$ (bottom)

	$[LBPh_2]^{2-}$	expt	calc		$[^{H}LBPh_2]^{2-}$	expt	calc	
	($\mathbf{2}^{2-}$)		6-ring	5-ring	($^{\mathbf{H}}\mathbf{3}^{-}$)		6-ring	5-ring
^{13}C NMR	NCN	152.71	150.5	164.6	NCN	138.48	144.9	162.2
^{1}H NMR	Ph p-H	5.85	5.98	6.11	Ph p-H	6.12	6.49	6.46
				5.50		6.08	6.60	6.78
					N-H	5.04	4.84	4.85

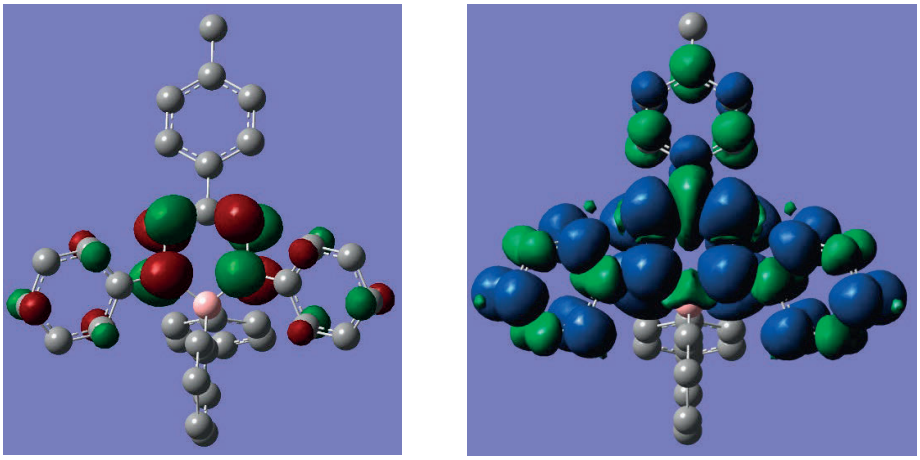

Figure S3.11 SOMO (left) and spin density plot (right) of $\mathbf{2}^{\cdot-}$

3.6 References

(1) Cook, T. R.; Dogutan, D. K.; Reece, S. Y.; Surendranath, Y.; Teets, T. S.; Nocera, D. G. *Chem. Rev.* **2010**, *110* (11), 6474.

(2) Appel, A. M.; Bercaw, J. E.; Bocarsly, A. B.; Dobbek, H.; DuBois, D. L.; Dupuis, M.; Ferry, J. G.; Fujita, E.; Hille, R.; Kenis, P. J. A.; Kerfeld, C. A.; Morris, R. H.; Peden, C. H. F.; Portis, A. R.; Ragsdale, S. W.; Rauchfuss, T. B.; Reek, J. N. H.; Seefeldt, L. C.; Thauer, R. K.; Waldrop, G. L. *Chem. Rev.* **2013**, *113* (8), 6621.

(3) (a) Klerke, A.; Christensen, C. H.; Norskov, J. K.; Vegge, T. *J. Mater. Chem.* **2008**, *18* (20), 2304. (b) Schuth, F.; Palkovits, R.; Schlogl, R.; Su, D. S. *Energy Environ. Sci.* **2012**, *5* (4), 6278.

(4) Roger, I.; Shipman, M. A.; Symes, M. D. *Nat. Rev. Chem.* **2017**, *1*, 0003.

(5) Blakemore, J. D.; Crabtree, R. H.; Brudvig, G. W. *Chem. Rev.* **2015**, *115* (23), 12974.

(6) (a) Whittaker, J. W. *Chem. Rev.* **2003**, *103* (6), 2347. (b) Lyons, C. T.; Stack, T. D. P. *Coord. Chem. Rev.* **2013**, *257* (2), 528.

(7) Rittle, J.; Green, M. T. *Science* **2010**, *330* (6006), 933.

(8) (a) Dzik, W. I.; van der Vlugt, J. I.; Reek, J. N. H.; de Bruin, B. *Angew. Chem. Int. Ed.* **2011**, *50* (15), 3356. (b) Lyaskovskyy, V.; de Bruin, B. *ACS Catal.* **2012**, *2* (2), 270. (c) Luca, O. R.; Crabtree, R. H. *Chem. Soc. Rev.* **2013**, *42* (4), 1440. (d) Broere, D. L. J.; Plessius, R.; van der Vlugt, J. I. *Chem. Soc. Rev.* **2015**, *44* (19), 6886.

(9) (a) Römelt, C.; Song, J.; Tarrago, M.; Rees, J. A.; van Gastel, M.; Weyhermüller, T.; DeBeer, S.; Bill, E.; Neese, F.; Ye, S. *Inorg. Chem.* **2017**, *56* (8), 4745. (b) Römelt, C.; Ye, S.; Bill, E.; Weyhermüller, T.; van Gastel, M.; Neese, F. *Inorg. Chem.* **2018**, *DOI: 10.1021/acs.inorgchem.7b03018*.

(10) Wu, Y.; Jiang, J.; Weng, Z.; Wang, M.; Broere, D. L. J.; Zhong, Y.; Brudvig, G. W.; Feng, Z.; Wang, H. *ACS Cent. Sci.* **2017**, *3* (8), 847.

(11) (a) Sengupta, D.; Bhattacharjee, R.; Pramanick, R.; Rath, S. P.; Saha Chowdhury, N.; Datta, A.; Goswami, S. *Inorg. Chem.* **2016**, *55* (19), 9602. (b) Sinha, S.; Das, S.; Sikari, R.; Parua, S.; Brandaõ, P.; Demeshko, S.; Meyer, F.; Paul, N. D. *Inorg. Chem.* **2017**, *56* (22), 14084.

(12) Schilter, D.; Camara, J. M.; Huynh, M. T.; Hammes-Schiffer, S.; Rauchfuss, T. B. *Chem. Rev.* **2016**, *116* (15), 8693.

(13) Dempsey, J. L.; Brunschwig, B. S.; Winkler, J. R.; Gray, H. B. *Acc. Chem. Res.* **2009**, *42* (12), 1995.

(14) Kaeffer, N.; Chavarot-Kerlidou, M.; Artero, V. *Acc. Chem. Res.* **2015**, *48* (5), 1286.

(15) (a) Bhattacharjee, A.; Chavarot-Kerlidou, M.; Andreiadis, E. S.; Fontecave, M.; Field, M. J.; Artero, V. *Inorg. Chem.* **2012**, *51* (13), 7087. (b) Estes, D. P.; Grills, D. C.; Norton, J. R. *J. Am. Chem. Soc.* **2014**, *136* (50), 17362. (c) Lacy, D. C.; Roberts, G. M.; Peters, J. C. *J. Am. Chem. Soc.* **2015**, *137* (14), 4860.

(16) Wiedner, E. S.; Bullock, R. M. *J. Am. Chem. Soc.* **2016**, *138* (26), 8309.

(17) (a) Wilson, A. D.; Newell, R. H.; McNevin, M. J.; Muckerman, J. T.; Rakowski DuBois, M.; DuBois, D. L. *J. Am. Chem. Soc.* **2006**, *128* (1), 358. (b) Helm, M. L.; Stewart, M. P.; Bullock, R. M.; DuBois, M. R.; DuBois, D. L. *Science* **2011**, *333* (6044), 863. (c) Bullock, R. M.; Appel, A. M.; Helm, M. L. *Chem. Commun.* **2014**, *50* (24), 3125.

(18) (a) McNamara, W. R.; Han, Z.; Alperin, P. J.; Brennessel, W. W.; Holland, P. L.; Eisenberg, R. *J. Am. Chem.*

Soc. **2011**, *133* (39), 15368. (b) McNamara, W. R.; Han, Z.; Yin, C.-J.; Brennessel, W. W.; Holland, P. L.; Eisenberg, R. *PNAS* **2012**, *109* (39), 15594.

(19) (a) Zarkadoulas, A.; Field, M. J.; Papatriantafyllopoulou, C.; Fize, J.; Artero, V.; Mitsopoulou, C. A. *Inorg. Chem.* **2016**, *55* (2), 432. (b) Zarkadoulas, A.; Field, M. J.; Artero, V.; Mitsopoulou, C. A. *ChemCatChem* **2017**, *9* (12), 2308.

(20) Lee, K. J.; McCarthy, B. D.; Rountree, E. S.; Dempsey, J. L. *Inorg. Chem.* **2017**, *56* (4), 1988.

(21) (a) Downes, C. A.; Marinescu, S. C. *J. Am. Chem. Soc.* **2015**, *137* (43), 13740. (b) Eady, S. C.; MacInnes, M. M.; Lehnert, N. *Inorg. Chem.* **2017**, *56* (19), 11654.

(22) (a) Solis, B. H.; Hammes-Schiffer, S. *J. Am. Chem. Soc.* **2012**, *134* (37), 15253. (b) Letko, C. S.; Panetier, J. A.; Head-Gordon, M.; Tilley, T. D. *J. Am. Chem. Soc.* **2014**, *136* (26), 9364. (c) Panetier, J. A.; Letko, C. S.; Tilley, T. D.; Head-Gordon, M. *J. Chem. Theory Comput.* **2016**, *12* (1), 223.

(23) (a) Haddad, A. Z.; Kumar, D.; Ouch Sampson, K.; Matzner, A. M.; Mashuta, M. S.; Grapperhaus, C. A. *J. Am. Chem. Soc.* **2015**, *137* (29), 9238. (b) Zhang, W.; Haddad, A. Z.; Garabato, B. D.; Kozlowski, P. M.; Buchanan, R. M.; Grapperhaus, C. A. *Inorg. Chem.* **2017**, *56* (4), 2177. (c) Haddad, A. Z.; Cronin, S. P.; Mashuta, M. S.; Buchanan, R. M.; Grapperhaus, C. A. *Inorg. Chem.* **2017**, *56* (18), 11254.

(24) (a) Solis, B. H.; Maher, A. G.; Dogutan, D. K.; Nocera, D. G.; Hammes-Schiffer, S. *PNAS* **2016**, *113* (3), 485. (b) Dempsey, J. L. *PNAS* **2016**, *113* (3), 478.

(25) (a) Thompson, E. J.; Berben, L. A. *Angew. Chem. Int. Ed.* **2015**, *54* (40), 11642. (b) Sherbow, T. J.; Fettinger, J. C.; Berben, L. A. *Inorg. Chem.* **2017**, *56* (15), 8651. (c) Haddad, A. Z.; Garabato, B. D.; Kozlowski, P. M.; Buchanan, R. M.; Grapperhaus, C. A. *J. Am. Chem. Soc.* **2016**, *138* (25), 7844. (d) Jiang, J.; Materna, K. L.; Hedström, S.; Yang, K. R.; Crabtree, R. H.; Batista, V. S.; Brudvig, G. W. *Angew. Chem. Int. Ed.* **2017**, *56* (31), 9111. (e) For a review on main group compounds showing transition metal-like reactivity, see: Power, P. P. *Nature* **2010**, *463*, 171

(26) (a) Gilroy, J. B.; Ferguson, M. J.; McDonald, R.; Patrick, B. O.; Hicks, R. G. *Chem. Commun.* **2007** (2), 126. (b) Gilroy, J. B.; Ferguson, M. J.; McDonald, R.; Hicks, R. G. *Inorg. Chim. Acta* **2008**, *361* (12-13), 3388. (c) Gilroy, J. B.; Patrick, B. O.; McDonald, R.; Hicks, R. G. *Inorg. Chem.* **2008**, *47* (4), 1287. (d) Gilroy, J. B.; Otieno, P. O.; Ferguson, M. J.; McDonald, R.; Hicks, R. G. *Inorg. Chem.* **2008**, *47* (4), 1279. (e) Hong, S.; Hill, L. M. R.; Gupta, A. K.; Naab, B. D.; Gilroy, J. B.; Hicks, R. G.; Cramer, C. J.; Tolman, W. B. *Inorg. Chem.* **2009**, *48* (10), 4514.

(27) Chang, M.-C.; Dann, T.; Day, D. P.; Lutz, M.; Wildgoose, G. G.; Otten, E. *Angew. Chem. Int. Ed.* **2014**, *53* (16), 4118.

(28) For a review, see: Sigeikin, G. I.; Lipunova, G. N.; Pervova, I. G. Formazans and their metal complexes *Russ. Chem. Rev.* **2006**, *75*, 885.

(29) (a) Beffa, F.; Lienhard, P.; Steiner, E.; Schetty, G. *Helv. Chim. Acta* **1963**, *46* (4), 1369. (b) Dale, D. *J. Chem. Soc. A* **1967**, 278. (c) Balt, S.; Renkema, W. E. *J. Coord. Chem.* **1977**, *6* (4), 201. (d) Renkema, W. E.; Lute, C. N.; Stam, C. H. *Acta Cryst. B* **1979**, *35* (1), 75. (e) Balt, S.; Meuldijk, J.; Renkema, W. *Transition Met. Chem.* **1980**, *5* (1), 357. (f) Siedle, A. R.; Pignolet, L. H. *Inorg. Chem.* **1980**, *19* (7), 2052. (g) Jameson, G. B.; Muster, A.; Robinson, S. D.; Wingfield, J. N.; Ibers, J. A. *Inorg. Chem.* **1981**, *20* (8), 2448. (h) Meuldijk, J.; Renkema, W. E.; van Herk, A. M.; Stam, C. H. *Acta Cryst. C* **1983**, *39* (11), 1536. (i) Kawamura, Y.; Yamauchi, J. *Bull. Chem. Soc. Jpn.* **1995**, *68* (11), 3041. (j) Zhang, H.-Y.; Sun, W.-X.; Wu, Q.-A.; Zhangb, H.-Q.; Chen, Y.-Y. *Synth. React. Inorg. Met.-Org. Chem.* **2000**, *30* (4), 571. (k) Frolova,

N.; Vatsadze, S.; Zavodnik, V.; Rakhimov, R.; Zyk, N. *Russ. Chem. Bull.* **2006**, *55* (10), 1810.

(30) (a) Barbon, S. M.; Reinkeluers, P. A.; Price, J. T.; Staroverov, V. N.; Gilroy, J. B. *Chem. Eur. J.* **2014**, *20* (36), 11340. (b) Barbon, S. M.; Price, J. T.; Reinkeluers, P. A.; Gilroy, J. B. *Inorg. Chem.* **2014**, *53* (19), 10585. (c) Maar, R. R.; Barbon, S. M.; Sharma, N.; Groom, H.; Luyt, L. G.; Gilroy, J. B. *Chem. Eur. J.* **2015**, *21* (44), 15589. (d) Hesari, M.; Barbon, S. M.; Staroverov, V. N.; Ding, Z.; Gilroy, J. B. *Chem. Commun.* **2015**, *51* (18), 3766. (e) Barbon, S. M.; Staroverov, V. N.; Gilroy, J. B. *J. Org. Chem.* **2015**, *80* (10), 5226. (f) Barbon, S. M.; Price, J. T.; Yogarajah, U.; Gilroy, J. B. *RSC Advances* **2015**, *5* (69), 56316. (g) Maar, R. R.; Gilroy, J. B. *J. Mat. Chem. C* **2016**, *4* (27), 6478. (h) Maar, R. R.; Rabiee Kenaree, A.; Zhang, R.; Tao, Y.; Katzman, B. D.; Staroverov, V. N.; Ding, Z.; Gilroy, J. B. *Inorg. Chem.* **2017**, *56* (20), 12436. (i) Barbon, S. M.; Staroverov, V. N.; Gilroy, J. B. *Angew. Chem. Int. Ed.* **2017**, *56* (28), 8173. (j) Barbon, S. M.; Buddingh, J. V.; Maar, R. R.; Gilroy, J. B. *Inorg. Chem.* **2017**, *56* (19), 12003.

(31) (a) Tezcan, H.; Uzluk, E.; Aksu, M. L. *Electrochim. Acta* **2008**, *53* (18), 5597. (b) Zaidman, A. V.; Pervova, I. G.; Vilms, A. I.; Belov, G. P.; Kayumov, R. R.; Slepukhin, P. A.; Lipunov, I. N. *Inorg. Chim. Acta* **2011**, *367* (1), 29. (c) Protasenko, N. A.; Poddel'sky, A. I.; Bogomyakov, A. S.; Fukin, G. K.; Cherkasov, V. K. *Inorg. Chem.* **2015**. (d) Mandal, A.; Schwederski, B.; Fiedler, J.; Kaim, W.; Lahiri, G. K. *Inorg. Chem.* **2015**, *54* (16), 8126. (e) Kabir, E.; Wu, C.-H.; Wu, J. I. C.; Teets, T. S. *Inorg. Chem.* **2016**, *55* (2), 956. (f) Schorn, W.; Grosse-Hagenbrock, D.; Oelkers, B.; Sundermeyer, J. *Dalton Trans.* **2016**, *45* (3), 1201.

(32) (a) Novoa, S.; Paquette, J. A.; Barbon, S. M.; Maar, R. R.; Gilroy, J. B. *J. Mat. Chem. C* **2016**, *4* (18), 3987. (b) Barbon, S. M.; Gilroy, J. B. *Polymer Chem.* **2016**, *7* (21), 3589. (c) Barbon, S. M.; Novoa, S.; Bender, D.; Groom, H.; Luyt, L. G.; Gilroy, J. B. *Org. Chem. Front.* **2017**, *4* (2), 178. (d) Novoa, S.; Gilroy, J. B. *Polymer Chem.* **2017**, *8* (35), 5388.

(33) (a) Chang, M. C.; Otten, E. *Chem. Commun.* **2014**, *50* (56), 7431. (b) Chang, M. C.; Chantzis, A.; Jacquemin, D.; Otten, E. *Dalton Transactions* **2016**, *45* (23), 9477. (c) Mondol, R.; Snoeken, D. A.; Chang, M.-C.; Otten, E. *Chem. Commun.* **2017**, *53* (3), 513.

(34) Chang, M.-C.; Otten, E. *Inorg. Chem.* **2015**, *54* (17), 8656.

(35) (a) Matuschek, D.; Eusterwiemann, S.; Stegemann, L.; Doerenkamp, C.; Wibbeling, B.; Daniliuc, C. G.; Doltsinis, N. L.; Strassert, C. A.; Eckert, H.; Studer, A. *Chem. Sci.* **2015**, *6* (8), 4712. (b) Hicks, R. G. In *Stable Radicals*; John Wiley & Sons, Ltd: 2010, p 245.

(36) Chang, M.-C.; Otten, E. *Organometallics* **2016**, *35* (4), 534.

(37) Johnston, C. W.; Schwantje, T. R.; Ferguson, M. J.; McDonald, R.; Hicks, R. G. *Chem. Commun.* **2014**, *50* (83), 12542.

(38) (a) Polumbrik, O.; Ryabokon, I. *Zh. Org. Khim.* **1978**, *14* (6), 1332. (b) Misyura, A.; Polumbrik, O.; Markovskii, L. *Zh. Org. Khim.* **1989**, *25* (2), 424.

(39) Warren, J. J.; Tronic, T. A.; Mayer, J. M. *Chem. Rev.* **2010**, *110* (12), 6961.

(40) (a) Skene, W. G.; Belt, S. T.; Connolly, T. J.; Hahn, P.; Scaiano, J. C. *Macromolecules* **1998**, *31* (25), 9103. (b) Marque, S.; Le Mercier, C.; Tordo, P.; Fischer, H. *Macromolecules* **2000**, *33* (12), 4403.

(41) Lukkarila, J. L. PhD thesis, University of Toronto, 2009.

(42) (a) Marsal, P.; Roche, M.; Tordo, P.; de Sainte Claire, P. *J. Phys. Chem. A* **1999**, *103* (15), 2899. (b) Gaudel-Siri, A.; Siri, D.; Tordo, P. *ChemPhysChem* **2006**, *7* (2), 430.

(43) Huang, K.-W.; Han, J. H.; Cole, A. P.; Musgrave, C. B.; Waymouth, R. M. *J. Am. Chem. Soc.* **2005**, *127* (11), 3807.

(44) Ernst, R. R.; Bodenhausen, G.; Wokaun, A. *Clarendon Press*; Oxford, 1987, p. 490.

(45) Goddard, T. D.; Kneller, D. G. *SPARKY 3*, University of California, San Francisco.

(46) Wolfram Research, Inc., Mathematica 10.3, Champaign, I. (2016).

(47) *Gaussian 09, Revision D.01,* M. J. Frisch, G. W. Trucks, H. B. Schlegel, G. E. Scuseria, M. A. Robb, J. R. Cheeseman, G. Scalmani, V. Barone, B. Mennucci, G. A. Petersson, H. Nakatsuji, M. Caricato, X. Li, H. P. Hratchian, A. F. Izmaylov, J. Bloino, G. Zheng, J. L. Sonnenberg, M. Hada, M. Ehara, K. Toyota, R. Fukuda, J. Hasegawa, M. Ishida, T. Nakajima, Y. Honda, O. Kitao, H. Nakai, T. Vreven, J. A. Montgomery, Jr., J. E. Peralta, F. Ogliaro, M. Bearpark, J. J. Heyd, E. Brothers, K. N. Kudin, V. N. Staroverov, R. Kobayashi, J. Normand, K. Raghavachari, A. Rendell, J. C. Burant, S. S. Iyengar, J. Tomasi, M. Cossi, N. Rega, J. M. Millam, M. Klene, J. E. Knox, J. B. Cross, V. Bakken, C. Adamo, J. Jaramillo, R. Gomperts, R. E. Stratmann, O. Yazyev, A. J. Austin, R. Cammi, C. Pomelli, J. W. Ochterski, R. L. Martin, K. Morokuma, V. G. Zakrzewski, G. A. Voth, P. Salvador, J. J. Dannenberg, S. Dapprich, A. D. Daniels, Ö. Farkas, J. B. Foresman, J. V. Ortiz, J. Cioslowski, and D. J. Fox, Gaussian, Inc., Wallingford CT, 2009.

(48) *GaussView, Version 5,* Dennington, Roy; Keith, Todd; Millam, John. *Semichem Inc.*, Shawnee Mission, KS, 2009.

(49) Marenich, A. V; Cramer, C. J.; Truhlar, D. G. *J. Phys. Chem. B* **2009**, *113* (18), 6378–6396.